View metadata, citation and similar papers at core.ac.uk

brought to you by CORE

provided by Elsevier - Publisher Connector

Procedia Manufacturing

Volume 1, 2015, Pages 355–365

43rd Proceedings of the North American Manufacturing Research Institution of SME http://www.sme.org/namrc

Fast Prediction and Validation of Part Distortion in Selective Laser Melting

C. Li[1], C.H. Fu[1], Y.B. Guo[1*], F.Z. Fang[2]

[1] *Dept. of Mechanical Engineering, The University of Alabama, Tuscaloosa, AL 35487, USA*

[2] *Center of MicroNano Manufacturing Technology, Tianjin University, 300072, China*

Abstract

Selective laser melting (SLM) is a powder bed based additive manufacturing process. It is widely used to make functional parts in a layer upon layer fashion. The high-temperature process will produce large tensile residual stress which leads to part distortion and negatively affect product performance. Due to the complex process mechanism and coupling multiscale phenomena, traditional modeling approaches are not practical to predict part distortion since it demands an exceedingly long computational time. This study has developed a practical multiscale finite element model for fast prediction of distortion of SLMed parts with four laser scanning strategies. The predicted part distortions were validated with experimental data.

Keywords: Selective laser melting, distortion, laser scanning strategy, FEA

1 Introduction

Selective laser melting (SLM) is a powder bed based additive manufacturing process. It is able to produce functional parts from CAD data in a layer upon layer fashion (Kruth et al., 1998; Levy et al., 2003). Parts produced by SLM have near full density with comparable mechanical properties to bulk material (Kruth et al., 2007; Kruth et al., 2004). SLM is widely used in aerospace, automotive, and biomedical industries (Vandenbroucke & Kruth, 2007; Clare et al., 2008; Hollander et al., 2006; Rochus et al., 2007).

During a typical SLM process, a fine powder delivering system is used to place a 20 μm to 100 μm thick powder layer onto a substrate plate inside a building chamber with an inert atmosphere. In order to achieve near full density, a laser is used to fully melt the powder materials. During the melting process, energy and mass transformation occurs through various physical phenomena, such as absorption and scattering of laser radiation, heat transfer, and fluid flow within the molten pool. High temperature gradient due to rapid heating and cooling generates thermal stress and leads to cracks and

* Corresponding author
Tel.: 1-205-348-2615; fax: +1-205-348-6419. E-mail address: yguo@eng.ua.edu

2351-9789 © 2015 The Authors. Published by Elsevier B.V. This is an open access article under the CC BY-NC-ND license (http://creativecommons.org/licenses/by-nc-nd/4.0/).

Peer-review under responsibility of the NAMRI Scientific Committee
doi:10.1016/j.promfg.2015.09.042

part distortion (Shiomi et al., 2004). High viscosity of molten powder materials makes the molten pool break apart into small balls, also known as balling effect, which results in deteriorated surface finish and porosity (Li et al., 2012; Gu & Shen, 2007). Surface tension could be another contributing factor to balling.

Part distortion due to residual stress is one of the major defects of SLM parts. It reduces the part geometrical accuracy and detrimentally affects the performance of the end-use parts. Numerical modeling as a powerful tool has been widely used to predict part residual stress and distortion. However, traditional thermal-mechanical modeling techniques demand large amount of computational time for a practical macro-scale SLM part. Numerous simulations (Li et al., 2004; Nickel et al., 2001; Hodge et al., 2013; Aggarangsi & Beuth, 2006; Dai & Shaw, 2001) have been done to predict residual stress and distortion of SLM parts only on a micro-scale level. The coupled thermal-mechanical analysis for several layers at micrometer level with a fine mesh was very time consuming, ranging from hours to days. It is very challenging to predict a practical SLM part using this method. Some studies (Zaeh & Branner, 2010; Krol et al., 2011; Papadakis et al., 2013) predicted residual stress and part distortion in SLM on a macro-scale. The modeling approaches were based on applying a uniform thermal load to one layer or multiple layers at one time. Moreover, no scanning strategy was taken into consideration. However, it should be noted that a uniform thermal load applied on one layer or multiple layers underestimates the steep temperature gradient in SLM process. Furthermore, scanning strategy plays an important role in temperature distribution, part distortion, and cracks formation in SLM parts (Yasa et al., 2009; Beal et al., 2008). However, little has been done to address the aforementioned aspects.

Therefore, the objective of this study is to develop a practical finite element model for fast prediction of SLM part distortion by (a) developing a novel equivalent heat source that includes temperature gradient within single pass microscale laser scanning, (b) calculating a local residual stress field in a meso-scale hatch area, (c) mapping residual stress field into a macroscale part model with four scanning strategies, and (d) validating the predicted distortion with experimental data.

2 Simulation Conditions

The laser source in this study is a continuous Nd:YAG laser with a wavelength of 1.064 μm. The process parameters including laser power, laser spot diameter, scan speed, scan spacing, and layer thickness are listed in Table 1.

Table 1 SLM process parameters

Laser power W	Laser spot diameter μm	Scan speed mm/s	Scan spacing μm	Layer thickness μm
300	600	50	100	150

This study is to predict the part distortion and compare with the experimental data with lab-made iron-based powders (Kruth et al., 2004). A steel-based commercial material from EOS GmbH named DirectSteel® is used to approximate the iron-based powders. The comparison between the iron-based powder and DirectSteel® is listed in Table 2. Temperature-independent mechanical and thermal material properties of DirectSteel® are listed in Table 3. The substrate is a steel plate.

Table 2 Comparison of chemical composition between iron-based powder (Kruth et al., 2004) and DirectSteel®(Rombouts et al., 2006)

Powder material	Fe wt.%	Ni wt.%	Cu wt.%	P wt.%	Ref.
Iron-based powder	62.66	20.00	15.00	2.34	(Kruth et al., 2004)
DirectSteel® powder	59.3 ± 0.4	29.1 ± 1.4	9.6 ± 0.9	1.5 ± 0.1	(Rombouts et al., 2006)

Table 3 Material properties of solid DirectSteel®(EOS GmbH, 2004)

Elastic Modulus	Poisson's ratio	Tensile strength	Yield strength
GPa	-	MPa	MPa
15.3	0.41	600	400
Melting point	Coefficient of thermal expansion	Thermal conductivity	Specific heat
^{o}C	10^{-6}/K	W/m·K	J/kg·K
1330	9	13	375

3 Simulation Methodology

In order to achieve reliable distortion prediction of SLM parts with reasonable computational time, a finite element model has been developed. First, a moving heat flux was applied on the surface of the powder material to calculate the temperature field of a stabilized molten pool in the micro-scale scan model. Second, an equivalent heat source was developed from the temperature field in the scan model and imported to the meso-scale hatch model to obtain a local residual stress field. Third, the residual stress field was extended to the macro-scale part model to predict part distortion with different scanning strategies. This methodology may be extended to a practical SLM part with complex shape or odd features. As long as the size of one hatch is small enough, the hatch can be used as a building block to transfer predefined stress field to part model. However, this study focuses on the fundamental method. A case for practical part with small geometrical feature will be explored in the future.

3.1 Temperature field in micro-scale laser scanning

In the micro-scale laser scanning simulation, the finite element analysis (FEA) package ABAQUS/Standard was used to conduct a thermal analysis to predict temperature field in the molten pool. The mesh is shown in Fig. 1. The model had two components: powder layer and substrate. The dimensions of the powder layer were 5 mm × 0.6 mm × 0.15 mm (length × width × thickness) and the dimensions of the substrate were 5 mm × 0.6 mm × 5 mm (length × width × height). The powder layer had a fine mesh with an element size of 50 μm × 50 μm × 37.5 μm (length × width × thickness). The laser scanning is symmetric with respect to X-Z plane to decrease the computational time. The initial temperature of powder and substrate is 20 °C. The powder material was heated by a moving surface heat flux with Gaussian distribution. One single track was scanned to obtain a continuous molten pool.

When the molten pool became stable i.e. no dimensional changes in width, depth, and length was observed; the temperature field on the cross-section of the stabilized molten pool was recorded, as shown in Fig. 2. An equivalent heat input was developed from the temperature field and applied to the subsequent meso-scale hatching layer to predict local residual stress. Every point at the same relative spatial location on the cross-section of melt pool along the scanning direction experiences similar temperature history, it is reasonable to extend the molten pool cross-section temperature field to the whole scan track.

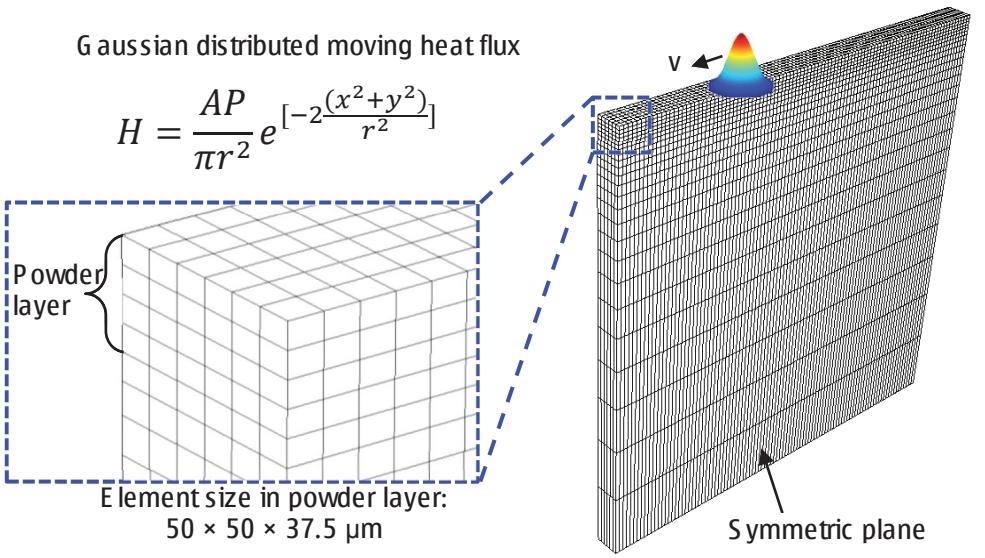

Fig. 1 Micro-scale laser scanning with moving Gaussian heat flux.

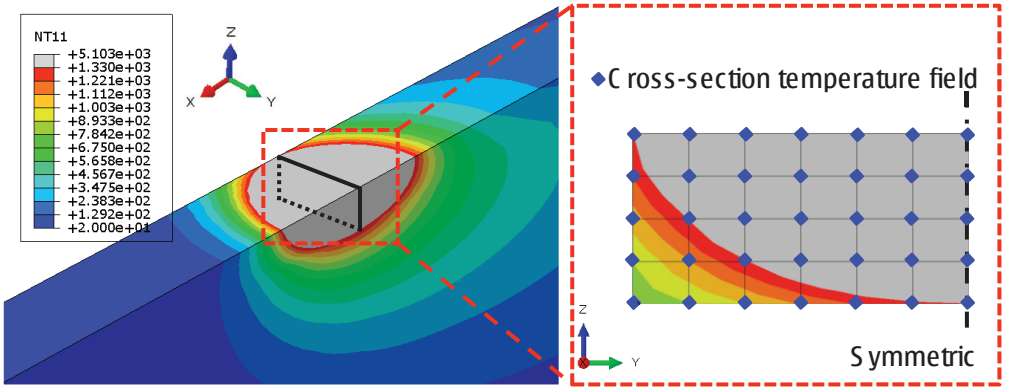

Fig. 2 Temperature field in the cross-section of laser scanning track.

3.2 Residual stress field in meso-scale hatch layer

In the meso-scale hatch layer, a coupled thermal-mechanical analysis was conducted to predict the local residual stress distribution. The detailed model dimensions with boundary conditions are shown in Fig. 3. Same mesh density and mesh size were used in the powder layer as the micro-scale laser scanning. The substrate bottom was fixed to provide proper constrain to the hatch layer.

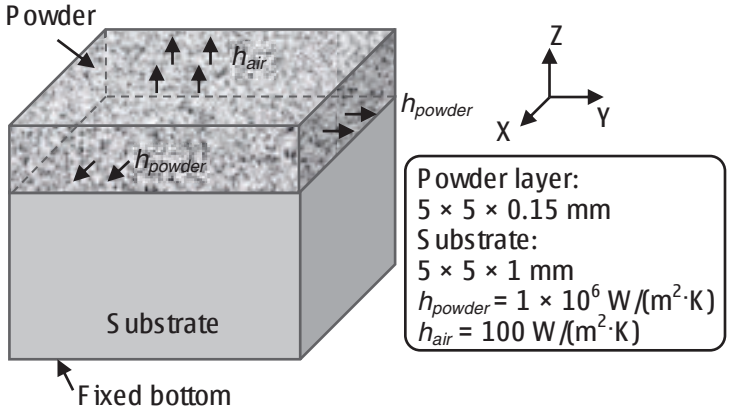

Fig. 3 Dimension and boundary conditions in the meso-scale hatch layer.

Multiple scans with the fixed scan spacing were achieved simultaneously by the equivalent heat input. The equivalent heat input was applied on the powder layer. Then, the powder and substrate were cooled down for 10 seconds to achieve a uniformly distributed temperature field around 20 °C. It was stated that heat lost by convection between molten pool and powder bed is significant in powder bed based additive manufacturing process (Dai & Shaw, 2004). Therefore, three cooling mechanisms are incorporated, namely, heat conduct to the substrate, heat convection from molten pool to powder bed and surrounding atmosphere, and heat radiated to the surrounding atmosphere. The residual stress predicted in the meso-scale hatch layer was imported to the subsequent macro-scale part model as a unit patch for distortion prediction.

3.3 Distortion of macro-scale part

In SLM, molten pool experiences a comparable mechanical history; therefore, it is feasible to fast predict the macro-scale part distortion by importing local stress field from the meso-scale hatch layer.

The mesh design of the macro-scale part model is shown in Fig. 4. The dimensions of the powder layer were 35 mm (length) × 15 mm (width) × 0.15 mm (thickness). The powder layer was placed on top of a steel plate that had a dimension of 45 mm (length) × 22 mm (width) × 1 mm (thickness). Within the fine mesh in the powder layer, the element size was 150 μm × 150 μm ×50 μm.

Different scanning strategies were studied in the macro-scale part, namely, (a) sequential pattern (horizontal scan), (b) sequential pattern (vertical scan), (c) successive pattern, and (d) least heat influence (LHI) pattern. Fig. 5 shows the four scanning patterns. For successive and LHI pattern, the scanning area was divided into 21 scan patches (5 mm × 5 mm). Number in each patch in Fig. 5 represents the laser scanning order.

The successive patches were laser scanned based on scanning sequence, an initial stress tensor was assigned to each element in the corresponding patch. If there is a rotation of laser scanning direction

between two successive patches, the residual stress tensor from the meso-scale hatch layer was rotated accordingly.

During the cooling process of the hatch layer, the side of the hatch layer is restrained by its surrounding material that is already solidified. It would be ideal to apply displacement boundary conditions to each side of the patch. However, this will make the simulation very complex and tedious and significantly increase computational cost. Even the hatch side is restraining, it would not significantly affect simulation accuracy as the hatch layer dimension is very small compared to the part dimension. In addition, the smaller the hatch layer size, the accurate the model prediction.

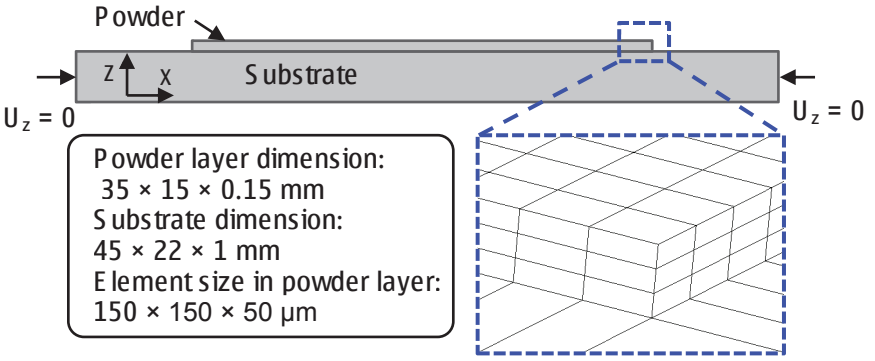

Fig. 4 Dimension and boundary conditions in the macro-scale part model.

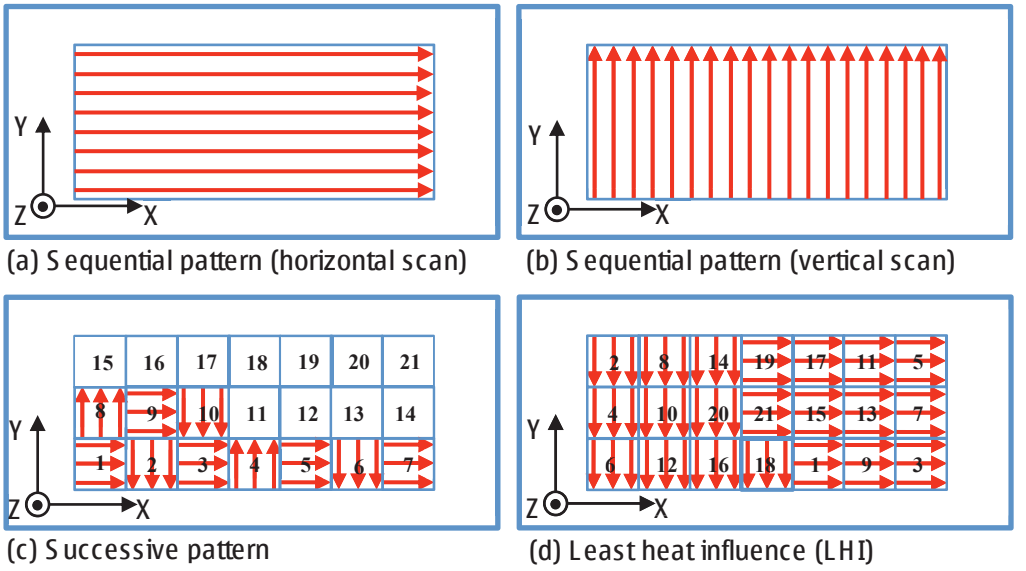

Fig. 5 Four scanning strategies (a) horizontal, (b) vertical, (c) successive, (d) LHI.

4 Model Validation and Discussions

4.1 Deflection in the hatch layer

Deflection predicted by the meso-scale hatch layer is shown in Fig. 6. At first, the top layers were heated, the expansion of the heated layer was restricted by the surrounding area; therefore, a compressive stress was generated on the top surface. When the yield stress of the material was reached, plastic bending occurs (t = 0 s). As the hatch layer cools down, the contraction of the top layer was then restricted by the surrounding area, leading to a tensile residual stress on the top surface. Also, the cooling and shrinkage created shorter top layers than the bottom layers, thus, the component was deflected by bending towards the laser beam. This predicted phenomenon agrees well with the temperature gradient mechanism (Fu & Guo, 2014).

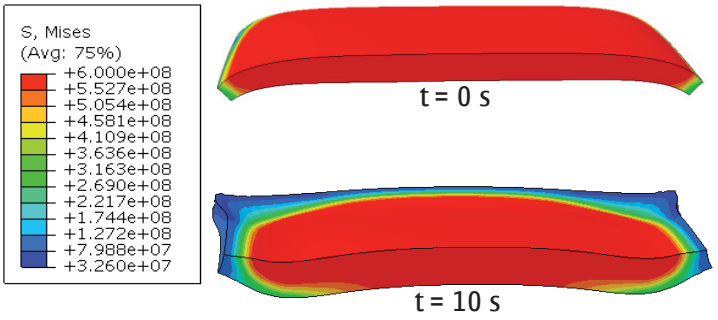

Fig. 6 Deflection in the meso-scale hatch layer (half-hatch shown due to symmetric).

4.2 Distortion of the macro parts

Longitudinal distortion of vertical scanning pattern vs. experimental result: A nodal path located at the back of the substrate along the longitudinal deflection direction (X) was created (see Fig.7). The distortion along this nodal path was normalized and compared to the experimental data (Fig. 7). Similar bending trend was observed for both prediction and measured data. This trend is attributed to the thermal history of the part. More specifically, the top layer was expanded at first due to the heat input. The plastic strain in the top layers became smaller than the bottom layers when cooling down. Therefore a concave up curve gradually formed.

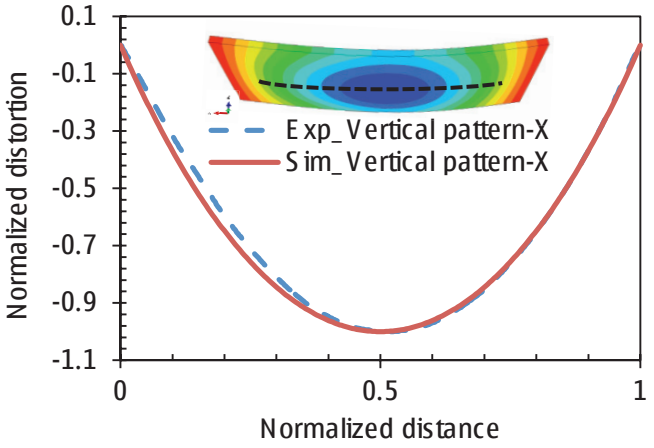

Fig. 7 Comparison between the predicted distortion and measured data.

Longitudinal distortion for different scanning strategies: Distortions along the longitudinal direction for four scanning strategies are shown in Fig. 8. It can be seen that the horizontal scanning pattern produced the smallest distortion in X direction, while the vertical scanning pattern resulted in the biggest distortion in X direction. Moreover, no significant difference in distortion along X direction was observed between the successive pattern and the LHI pattern. The distortion for the successive pattern is only slightly smaller than the LHI pattern. The possible reason for this difference is that a higher temperature gradient exists in the LHI scanning process than that in the successive scanning process.

Crosswise distortion for different scanning strategies: Distortions along the crosswise direction (Y) for the four scanning strategies are shown in Fig. 9. It can be found that the horizontal scanning pattern produced the biggest distortion in Y direction, while the vertical scanning pattern resulted in the smallest distortion in Y direction. For the successive and LHI patterns, same distortion trend was found as along longitudinal direction. The predicted distortions along the longitudinal (X) and crosswise (Y) directions for four scanning strategies were consistent with the experimental data (Kruth et al., 2004).

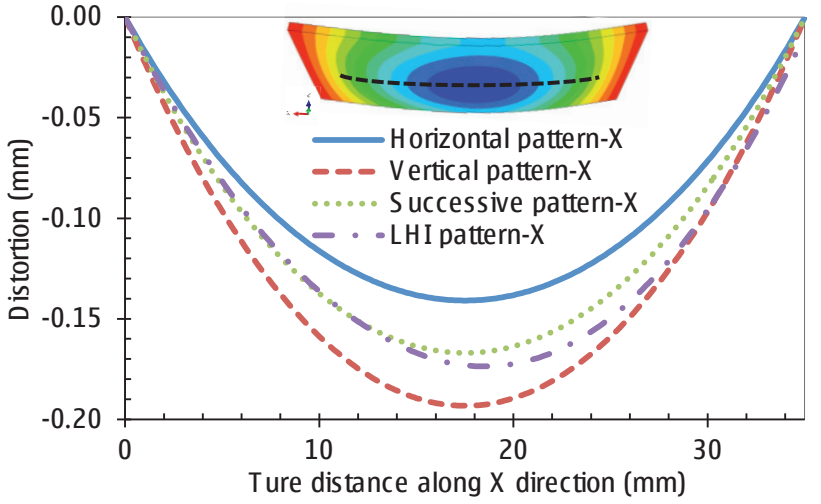

Fig. 8 Distortion along the longitudinal (X) direction for different scanning strategies.

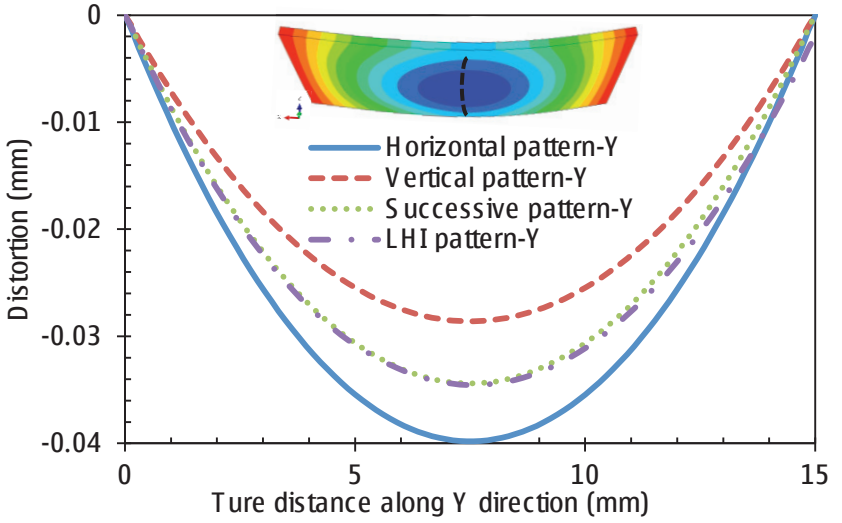

Fig. 9 Distortion along the crosswise (Y) direction for different scanning strategies.

According to the longitudinal and crosswise distortion patterns, smallest deflection occurs in the longitudinal direction. The reason is that the heat was more evenly distributed parallel to the scanning direction than the perpendicular direction.

5 Conclusions

A practical finite element model has been developed for fast prediction of part distortion in SLM. The predicted distortions in four different scanning strategies were investigated and verified by the experimental data. The key findings are summarized as follows:

- An equivalent heat source with temperature gradient has been developed from the micro-scale laser scanning and imported to the meso-scale hatch layer to predict local residual stress, which can be mapped into the macro-scale part to predict part distortion.
- The predicted part distortions showed that the horizontal scanning pattern produced the smallest deflection along longitudinal direction and the biggest deflection along crosswise direction. On the contrary, the vertical scanning pattern resulted in the biggest deflection along longitudinal direction and smallest deflection along crosswise direction.
- The successive scanning strategy is preferred to the LHI pattern in terms of reducing part distortion.

References

Aggarangsi, P., Beuth, J.L. (2006). Localized preheating approaches for reducing residual stress in additive manufacturing. *Proc. SFF Symp.*, Austin, 709-720.

Beal, V., Erasenthiran, P., Hopkinson, N., Dickens, P., Ahrens, C.H. (2008). Scanning strategies and spacing effect on laser fusion of H13 tool steel powder using high power nd: YAG pulsed laser. *International Journal of Production Research*, 46(1), 217-232.

Fu, C.H., Guo, Y.B. (2014). Three-dimensional temperature gradient mechanism in selective laser melting of Ti-6Al-4V. *Journal of Manufacturing Science and Engineering*, 136(6), 1004-1-1004-7.

Clare, A.T., Chalker, P.R., Davies, S., Sutcliffe, C.J., Tsopanos, S. (2008). Selective laser melting of high aspect ratio 3D nickel–titanium structures two way trained for MEMS applications. *International Journal of Mechanics and Materials in Design*, 4(2), 181-187.

Dai, K., Shaw, L. (2004). Thermal and mechanical finite element modeling of laser forming from metal and ceramic powders. *Acta Materialia*, 52(1), 69-80.

Dai, K., Shaw, L. (2001). Thermal and stress modeling of multi-material laser processing. *Acta Materialia*, 49(20), 4171-4181.

EOS GmbH (2004). Direct metal and DirectSteel materials for EOSINT M 250 xtended.

Gu, D., Shen, Y. (2007). Balling phenomena during direct laser sintering of multi-component Cu-based metal powder. *Journal of Alloys and Compounds*, 432(1), 163-166.

Hodge, N., Ferencz, R., Solberg, J. (2013). Implementation of a thermomechanical model in diablo for the simulation of selective laser melting. Lawrence Livermore National Laboratory (LLNL), Livermore, CA.

Hollander, D.A., Von Walter, M., Wirtz, T., Sellei, R., Schmidt-Rohlfing, B., Paar, O., Erli, H. (2006). Structural, mechanical and in vitro characterization of individually structured Ti–6Al–4V produced by direct laser forming. *Biomaterials*, 27(7), 955-963.

Krol, T., Westhäuser, S., Zaeh, M., Schilp, J. (2011). Development of a simulation-based process chain-strategy for different levels of detail for the preprocessing definitions. *Symposium Simulationstechnik*, Winterthur, ASIM 2011-21.

Kruth, J., Froyen, L., Van Vaerenbergh, J., Mercelis, P., Rombouts, M., Lauwers, B. (2004). Selective laser melting of iron-based powder. *Journal of Materials Processing Technology*, 149(1), 616-622.

Kruth, J., Leu, M., Nakagawa, T. (1998). Progress in additive manufacturing and rapid prototyping. *CIRP Annals-Manufacturing Technology*, 47(2), 525-540.

Kruth, J., Levy, G., Klocke, F., Childs, T. (2007). Consolidation phenomena in laser and powder-bed based layered manufacturing. *CIRP Annals-Manufacturing Technology*, 56(2), 730-759.

Levy, G.N., Schindel, R., Kruth, J. (2003). Rapid manufacturing and rapid tooling with layer manufacturing (LM) technologies, state of the art and future perspectives. *CIRP Annals-Manufacturing Technology*, 52(2), 589-609.

Li, R., Liu, J., Shi, Y., Wang, L., Jiang, W. (2012). Balling behavior of stainless steel and nickel powder during selective laser melting process. *The International Journal of Advanced Manufacturing Technology*, 59(9-12), 1025-1035.

Li, J.F., Li, L., Stott, F.H. (2004). Thermal stresses and their implication on cracking during laser melting of ceramic materials. *Acta Materialia*, 52(14), 4385-4398.

Nickel, A., Barnett, D., Prinz, F. (2001). Thermal stresses and deposition patterns in layered manufacturing. *Materials Science and Engineering: A*, 317(1), 59-64.

Papadakis, L., Loizou, A., Risse, J., Bremen, S. (2013). A thermo-mechanical modeling reduction approach for calculating shape distortion in SLM manufacturing for aero engine components. *Proceedings of the 6th International Conference on Advanced Research in Virtual and Rapid Prototyping*, Leiria, 1-5.

Rochus, P., Plesseria, J., Van Elsen, M., Kruth, J., Carrus, R., Dormal, T. (2007). New applications of rapid prototyping and rapid manufacturing (RP/RM) technologies for space instrumentation. *Acta Astronautica*, 61(1), 352-359.

Rombouts, M., Kruth, J.P., Froyen, L., Mercelis, P. (2006). Fundamentals of selective laser melting of alloyed steel powders. *CIRP Annals - Manufacturing Technology*, 55(1), 187-192.

Shiomi, M., Osakada, K., Nakamura, K., Yamashita, T., Abe, F. (2004). Residual stress within metallic model made by selective laser melting process. *CIRP Annals - Manufacturing Technology*, 53(1), 195-198.

Vandenbroucke, B., Kruth, J. (2007). Selective laser melting of biocompatible metals for rapid manufacturing of medical parts. *Rapid Prototyping Journal*, 13(4), 196-203.

Yasa, E., Deckers, J., Craeghs, T., Badrossamay, M., Kruth, J. (2009). Investigation on occurrence of elevated edges in selective laser melting. *Proc. SFF Symp.*, Austin, 673-685.

Zaeh, M.F., Branner, G. (2010). Investigations on residual stresses and deformations in selective laser melting. *Production Engineering,* 4(1), 35-45.